Seizure: European Journal of Epilepsy xxx (xxxx) xxx

Contents lists available at ScienceDirect

Seizure: European Journal of Epilepsy

journal homepage: www.elsevier.com/locate/seizure

Longitudinal changes in gray and white matter microstructure during epileptogenesis in pilocarpine-induced epileptic rats

Hiram Luna-Munguia, Luis Marquez-Bravo, Luis Concha *

Departamento de Neurobiologia Conductual y Cognitiva, Instituto de Neurobiologia, Universidad Nacional Autonoma de Mexico, Campus UNAM-Juriquilla, 76230, Queretaro, Mexico

ARTICLE INFO

Keywords:
Temporal lobe epilepsy
Pilocarpine
Diffusion tensor imaging
Fimbria
Hippocampus

ABSTRACT

Purpose: Temporal lobe epilepsy is associated with tissue abnormalities of several gray and white matter structures that are reproduced in animal models. Few longitudinal studies have focused on the identification of structural differences during epileptogenesis. The diffusion tensor model is a useful tool for evaluating cell death, gliosis, and axonal plasticity in epileptic subjects. This study aimed to evaluate temporal tissue changes after experimental *status epilepticus* in an animal model of chronic temporal lobe epilepsy.

Methods: Systemic pilocarpine-induced *status epilepticus* in adult Sprague-Dawley rats. Animals were scanned using diffusion tensor imaging (DTI) at three time points: prior to *status epilepticus*, and 24 and 64 days post-induction (early and late chronic, respectively). Fractional anisotropy, apparent diffusion coefficient, axial diffusivity ($D_{\parallel}$), and radial diffusivity ($D_{\perp}$) were evaluated in white (fimbria, cingulum, corpus callosum, and internal capsule) and gray (dorsal hippocampus, dentate gyrus, and CA3) matter regions for the three time points. Histological assessment of neurodegeneration in Klüver-Barrera preparations from the same animals was performed.

Results: Significantly reduced volume of dorsal hippocampus and fimbria of the epileptic animals was observed already at 24 days post-*status epilepticus*. Progressive changes of DTI parameters in both the white and gray matter structures of the experimental group were also observed. Stained sections confirmed such alterations.

Conclusion: Our study revealed time-dependent diffusion changes in gray and white matter structures after pilocarpine-induced *status epilepticus*. The characterization of these alterations over time may be potential imaging markers for epileptogenesis.

1. Introduction

Diffusion-weighted magnetic resonance imaging (MRI) has provided a noninvasive insight into the microstructural characteristics of tissue and anatomical connectivity without exogenous contrast agents. In particular, the tensor model [1] has been extensively used in the field of epilepsy for assessing hippocampal cell death, gliosis, and even axonal plasticity in humans [2,3] and experimental animals [4–8]. One of the most commonly derived diffusion tensor imaging (DTI) measures is fractional anisotropy (FA), which may be interpreted as a marker to identify subtly disturbed white matter microstructure. In this sense, Arfanakis and co-workers [9] were the first to report reduced FA in the external capsule and corpus callosum in patients with TLE when compared to control subjects. Later clinical studies corroborated that white matter abnormalities were not limited to the temporal lobe or the hemisphere ipsilateral to seizure focus, affecting other structures such as fimbria-fornix, internal capsule, and cingulum [10–14]. Recently, a large collaborative analysis demonstrated that while other forms of epilepsy also show DTI abnormalities, they are considerably more profound and distributed in TLE patients [15]. To date, it is well-established that TLE involves temporal and extra-temporal structures attributable in part to the recurrent seizures and their propagation patterns [16,17]. However, the progressive pattern of microstructural alterations of white matter during clinical epileptogenesis using DTI has not been investigated.

During the last decade, few studies involving animal models of epilepsy and MRI have focused on the understanding of epileptogenesis *in vivo*. Laitinen et al. [4] acquired *in vivo* DTI data from the rat dentate gyrus following kainic acid- and pilocarpine-induced *status epilepticus* (*SE*) and showed increased FA in said region after such prolonged

* Corresponding author.
E-mail address: lconcha@unam.mx (L. Concha).

https://doi.org/10.1016/j.seizure.2021.02.011
Received 11 December 2020; Received in revised form 28 January 2021; Accepted 9 February 2021
Available online 13 February 2021

seizure activity, which was histologically associated with mossy fiber sprouting and axonal plasticity. Similarly, Parekh et al. [5] described FA changes in specific anatomical regions such as hippocampus, fimbria, fornix, parahippocampal gyrus, and thalamus in an animal model of chronic TLE. Interestingly, these changes were only observed in animals that developed spontaneous limbic seizures and were also correlated with mossy fiber sprouting. In another study, van Eijsden et al. [18] described how pilocarpine-induced *SE* in juvenile rats induces significant DTI abnormalities in corpus callosum and fimbria-fornix 4 and 8 weeks post-induction. However, time points earlier than four weeks were not investigated, and no correlation between DTI changes and spontaneous recurrent seizures development was investigated. More recently, Salo et al. [19], based on their previous *ex vivo* DTI work [6], performed an *in vivo* longitudinal study to analyze progressive DTI changes in the rat hippocampal formation after *SE*. Their results clearly show that high-resolution DTI can detect progressive changes in the dentate gyrus and specific sub-regions of CA3 during epileptogenesis in experimental models. In a mouse model of TLE, Janz et al. [7] showed that early DTI changes within the hippocampus are attributable to radial gliosis, although the temporal trajectory of white matter abnormalities was not evaluated. Given the idea that high-resolution DTI can be used for early identification and tracking of the epileptogenic process in mesial TLE, new animal models have emerged. In this sense, Wang et al. [8] used the methionine sulfoximine (MSO) brain infusion model of mesial TLE. Here, the continuous infusion of MSO into the entorhinal-hippocampal-amygdala area of the rats inhibits the astroglial enzyme glutamine synthetase and triggers recurrent seizures that increase in severity over weeks. Their results, in contrast to other studies, show significant FA changes (decreases and increases) in several white and gray matter areas both early and late in epileptogenesis.

Based on the previous reports, structural changes in certain brain regions are often observed in individuals with TLE and in animal models. However, in patients, it is complicated to study brain structural changes during the evolution into epilepsy. Therefore, animal models that mimic the behavioral and neurophysiological features of human epilepsy provide a good alternative. In this sense, the pilocarpine model appears to be highly isomorphic with the human disease and it has been extensively used since its first description almost 40 years ago [20–22]. However, few longitudinal studies focused on the identification of structural differences after *SE* in experimental animals have been performed. Therefore, the aim of this study was to evaluate the temporal changes in gray and white matter microstructure after experimental *SE* through DTI in an animal model of chronic TLE. Imaging findings were compared to histological assessment of neurodegeneration in Klüver-Barrera preparations from the same animals.

2. Material and methods

2.1. Animals

Animal procedures were approved by our Institutional Ethics Committee (Protocol #105A) in accordance with federal regulations (NOM-062-ZOO-1999).

Thirty-five-day-old male Sprague-Dawley rats were provided by our animal facility and maintained under a 12 h light/dark cycle with access to food and water *ad libitum*. All animals were acclimatized to the room conditions (20−22 °C, 50–60 % humidity) for at least 5 days before any experimental manipulation.

2.2. In vivo MRI

Acquisition protocols were carried out at the National Laboratory for Magnetic Resonance Imaging using a 7 T MRI scanner (Bruker Pharmascan 70/16US) interfaced to a Paravision 6.0.1 console (Bruker, Ettlingen, Germany). *In vivo* DTI and T2-imaging were acquired using a 72 mm inner-diameter volume coil for transmission and a rat head 2 × 2 surface array coil for reception (Bruker, Ettlingen, Germany).

Control (n = 8) and epileptic rats (n = 11) were scanned at three time points: 1) before *SE* (see below), 2) 24 days after induction, and 3) 64 days after induction. Animals were anesthetized with a 4% isoflurane/air mixture concentration; a 2 % mix was used to maintain anesthesia during image acquisition. Anesthesia was discontinued upon termination of the imaging session.

Data sets for DTI were acquired using an echo-planar imaging sequence with the following parameters: TR = 2250 ms, TE = 31.32 ms, NA = 4, slice thickness = 750 μm, FOV = 20 × 14 mm^2, matrix = 150 × 104, yielding in-plane resolution of 133 × 135 μm^2, scan time = 15 min. Diffusion-weighted images were acquired in forty unique directions (δ/Δ = 2.9/8.7 ms), each with two different b values (650 and 2000s/mm^2) along with 6 images without diffusion weighting. Immediately afterwards, a 3-min Fast low-angle shot (FLASH) scan was acquired with the following parameters: TR = 350 ms, TE = 2.4 ms, NA = 3, flip angle = 30°, FOV = 25 × 18 mm^2, matrix = 250 × 180 (100 μm in-plane resolution), slice thickness = 800 μm, number of slices = 20.

2.3. Image data processing

DWI data sets were denoised [23] and corrected for motion and eddy-current-induced distortions using linear transformations (12 degrees of freedom). The MRtrix 3.0 software package [24] was used to estimate the diffusion tensor, from which we obtained the corresponding eigenvalues (λ_1, λ_2, and λ_3). From these, we created quantitative maps of FA [25], apparent diffusion coefficient (ADC), axial diffusivity (*i.e.*, λ_1; $D_\parallel$), and radial diffusivity ($[\lambda_2 + \lambda_3]/2$; $D_\perp$). DTI parameters were analyzed using the principal diffusivity maps (aided by the non-diffusion weighted images) to manually outline regions of interest (ROIs) of the dorsal hippocampus (further subdivided into dentate gyrus and CA3), fimbria, cingulum, corpus callosum, and internal capsule for the three time points (Supplementary Figure). Volume of the hippocampus and fimbria were divided from the same ROIs.

2.4. Pilocarpine-induced SE

Rats were randomly assigned to either epileptic (n = 11) or sham control (n = 8) groups. Detailed methods are described in Luna-Munguia et al. [26]. Animals were allowed 7 days to recover.

The pilocarpine-treated animals were continuously video-monitored at three different time points: 1) from day 8–12 post-*SE* in order to identify the first spontaneous seizure, 2) during the early chronic phase (days 21–24 post-induction), and 3) during the late chronic phase (days 59–63 post-induction). Videos were analyzed offline, and generalized seizures with rearing and falling were identified by an observer blinded to the groups.

2.5. Brain extraction

After the final time point, randomly, three controls and six epileptic rats were deeply anesthetized using isoflurane inhalation and overdosed using an intraperitoneal injection of sodium pentobarbital. Animals were transcardially perfused with 0.9 % NaCl followed by 4% paraformaldehyde (PFA). The brains were removed from the skull and post-fixed in 4% PFA until the histological procedure.

2.6. Histology

Three brains per group were randomly chosen for histology. First, the brains were dehydrated in alcohol solutions in increasing concentration, and in xylene as a diaphaneizer. Then, brains were included in paraffin blocks for subsequent cutting. Coronal sections of 5 μm were obtained by using a rotary microtome (Leica, model RM2135), and were later stained according to the Klüver-Barrera technique. Here, the brain sections were subjected to a hydration process with alcohol solutions in decreasing

concentrations and incubated overnight in Klüver-Barrera dye solution at 60 °C. To differentiate white matter from gray matter, a lithium carbonate solution 0.05 % was used. Finally, a counterstain with cresyl violet was performed. Here, the slices were dehydrated with alcohol solutions in increasing concentrations and mounted with non-aqueous mounting medium (Entellan, Merck Millipore). The stained brain sections were observed using an optical microscope (Leica ICC50 HD).

2.7. Statistical analysis

Values are expressed as mean ± S.E.M. Since we did not find any statistical asymmetries in the metrics for the paired ROIs (assessed through paired *t*-tests), we averaged the left and right values for each structure. Then, we conducted a repeated measures analysis of variance (ANOVA) followed by a *post-hoc* Sidak test to compare each time point for both groups. Differences between groups were analyzed using an unpaired *t*-test. Statistical analysis was performed using GraphPad Prism 8. In all statistical comparisons, $p < 0.05$ was used as a criterion for significance.

3. Results

3.1. Convulsive seizures video monitoring

All animals employed in this study reached the pilocarpine-induced *SE*. To verify that these animals present the features of epilepsy development as extensively reported for the pilocarpine model [20–22], we performed behavioral monitoring at specific time points. For one week after the *SE* induction, the animals entered a latency state in which they were apparently well [27]. On the eighth day, animals were continuously video monitored for 5 days to identify the first spontaneous seizure. This occurred 8.2 ± 0.35 days (mean ± S.E.M., n = 11) after *SE*. Then, as previously described, seizures occurred in clusters and aggravated in time [28]. During the early chronic stage, the mean frequency of generalized seizures of the whole group was 6.9 ± 2.84 per day and the mean forelimb clonus duration until full recovery was 176.1 ± 29.8 s. By full recovery we refer to the loss of the immobile behavior and reinstatement of spontaneous exploration of the cage by moving the four paws. In the case of the late chronic stage, the mean frequency of generalized seizures of the whole group was 9.5 ± 3.3 per day and the mean forelimb clonus duration until full recovery was 246.5 ± 33.52 s, indicating progression of the disease.

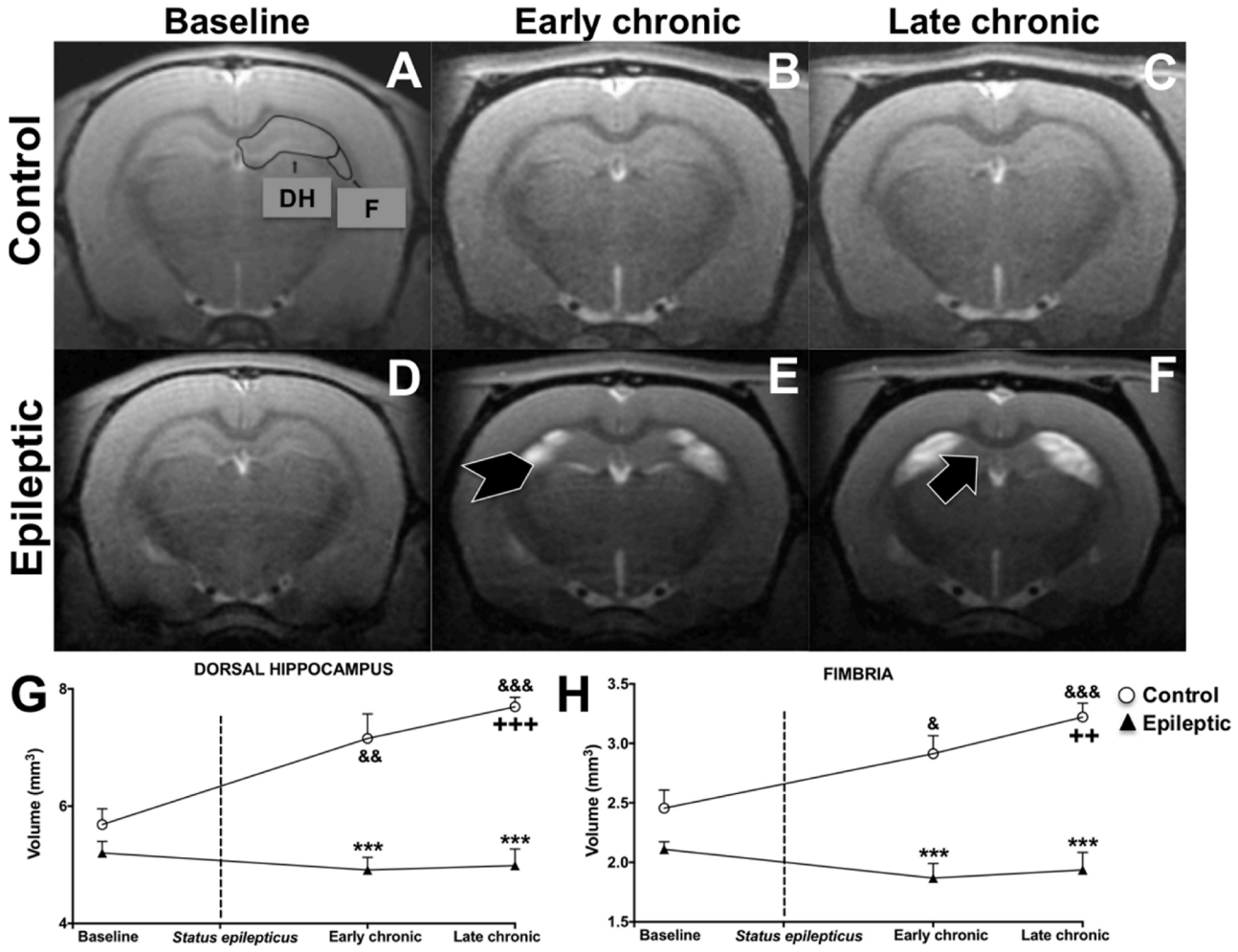

Fig. 1. Anatomical changes.
Representative coronal images in approximately the same slice from a Control (A-C) and an Epileptic (D-F) rat at different time points (DH: dorsal hippocampus; F: fimbria). The arrowhead in (E) shows enlargement of the ventricles 24 days post-*status epilepticus* induction, while the arrow in (F) points a significant reduction of the DH volume at 64 days post-induction. Quantitatively, the epileptic animals show reduced volume of dorsal hippocampus (G) and fimbria (H). + : repeated measures ANOVA; * : *post-hoc* between group differences; & : *post-hoc* within-group difference with respect to baseline (one, two or three symbols for $p < 0.05$, < 0.01, and < 0.001, respectively).

3.2. In vivo T2 changes

Fig. 1 shows gross bilateral alterations of the dorsal hippocampus and fimbria of epileptic animals. Specifically, there was a gradual enlargement of the ventricles from 24 days after the injection of pilocarpine (Fig. 1E) and a remarkable reduction of the dorsal hippocampal volume at 64 days post-induction (Fig. 1F). Quantitatively, there was significantly reduced volume of the dorsal hippocampus and fimbria of the epileptic animals at the early chronic phase (31 %, $p < 0.001$ and 36 %, $p < 0.001$, respectively) (Fig. 1G, H). Volumes further diverged between groups until the late chronic phase. Notably, only control animals showed progressive increases of volumes of both structures, while epileptic animals showed stagnant volumes over time (Fig. 1G, H).

3.3. In vivo DTI analysis

We investigated the progression of changes during the experiment, as well as differences between groups in each of the established time points (Baseline, 24 and 64 days post-*SE*).

3.3.1. White matter structures

The FA maps of the epileptic animals showed a sharp and significant reduction in the fimbria when compared to the respective control group references at both post-*SE* evaluations (Control Early chronic = 0.62 ± 0.021 and Epileptic Early chronic = 0.43 ± 0.018, $p < 0.001$; Control Late chronic = 0.67±0.013 and Epileptic Late chronic = 0.46±0.02, $p < 0.001$) (Fig. 2A). Longitudinal changes were observed in control (Baseline *vs* Late chronic, ↑13 %,

$p < 0.05$) and epileptic animals (Baseline *vs* Early (↓28 %) and Late

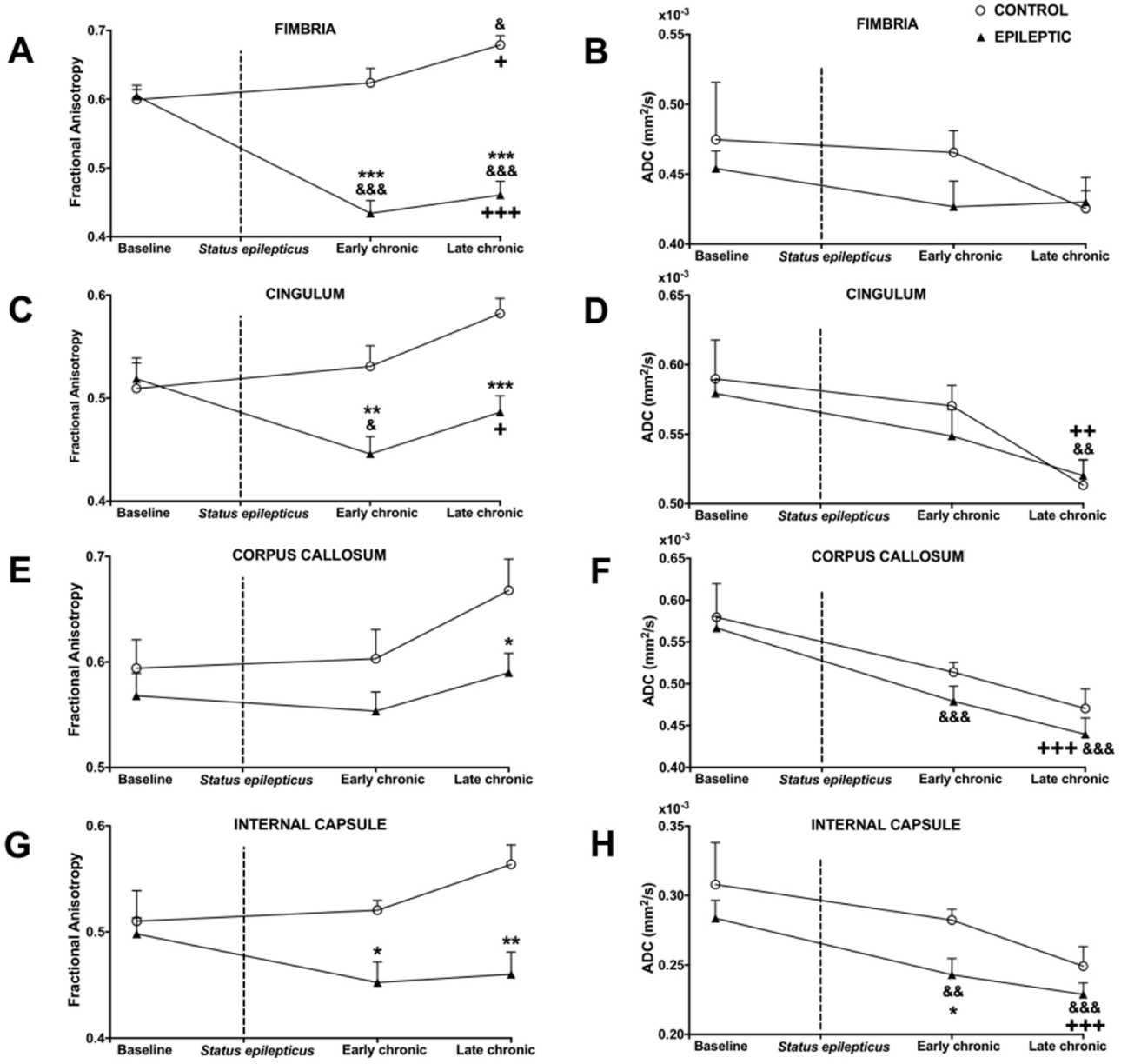

Fig. 2. Fractional anisotropy (FA) and apparent diffusion coefficient (ADC) values from white matter structures of Control and Epileptic rats.
Data obtained using *in vivo* DTI. The dotted line indicates the day of the pilocarpine-induced *status epilepticus*. The epileptic group shows significantly lower FA values when compared to the control group (A, C, E, G). Such differences are not so evident when comparing ADC values between groups (B, D, F, H). + : repeated measures ANOVA; * : *post-hoc* between group differences; & : *post-hoc* within-group difference with respect to baseline (one, two or three symbols for $p < 0.05$, < 0.01, and < 0.001, respectively).

chronic (↓24 %); both cases $p < 0.001$) (Fig. 2A). Regarding ADC, no significant changes between groups nor longitudinally were observed (Fig. 2B). Additionally, the epileptic animals showed decreased axial diffusivity ($D_{\parallel}$) at both post-induction time points in comparison to the control group (Control Early chronic = 0.85 ± 0.036 and Epileptic Early chronic = 0.64 ± 0.033, $p < 0.001$; Control Late chronic = 0.83±0.054 and Epileptic Late chronic = 0.66±0.02, $p < 0.01$) (Fig. 3A); longitudinally, only epileptic animals showed significant changes (Early chronic = ↓21 %, $p < 0.001$; Late chronic = 18 %, $p < 0.01$) (Fig. 3A). In contrast, the radial diffusivity ($D_{\perp}$) of the experimental group significantly increased with respect to the control animals at both post-induction measurements (Control Early chronic = 0.27 ± 0.013 and Epileptic Early chronic = 0.31 ± 0.013, $p < 0.05$; Control Late chronic = 0.22±0.008 and Epileptic Late chronic = 0.31±0.008, $p < 0.001$) (Fig. 3B); longitudinal changes were only observed in the control animals (Baseline *vs* Late chronic, ↓22 %, $p < 0.05$) (Fig. 3B).

In the case of the cingulum, FA values of epileptic animals significantly decreased at 24 days post-*SE* when compared to the control group, remaining abnormal in the next scan (Baseline = 0.51 ± 0.015; Early chronic = 0.44 ± 0.016 ($p < 0.01$); Late chronic = 0.48±0.015 ($p < 0.001$). Only the experimental group showed longitudinal statistical changes (Baseline *vs* Early chronic, ↓14 %, $p < 0.05$) (Fig. 2C). Regarding ADC, only longitudinal changes were observed in the epileptic animals (Baseline *vs* Late chronic, ↓10 %, $p < 0.01$) (Fig. 2D). A similar pattern was observed for $D_{\parallel}$, which also decreased in the epileptic animals (Baseline = 0.94 ± 0.026 and Early chronic = 0.82 ± 0.036; $p < 0.05$); longitudinal changes were only observed in the experimental animals (Early chronic = ↓11 %, $p < 0.05$; Late chronic = ↓13 %, $p < 0.05$) (Fig. 3C). On the other hand, while comparing $D_{\perp}$ values between groups, we noticed a significant change in the last time point (Baseline =

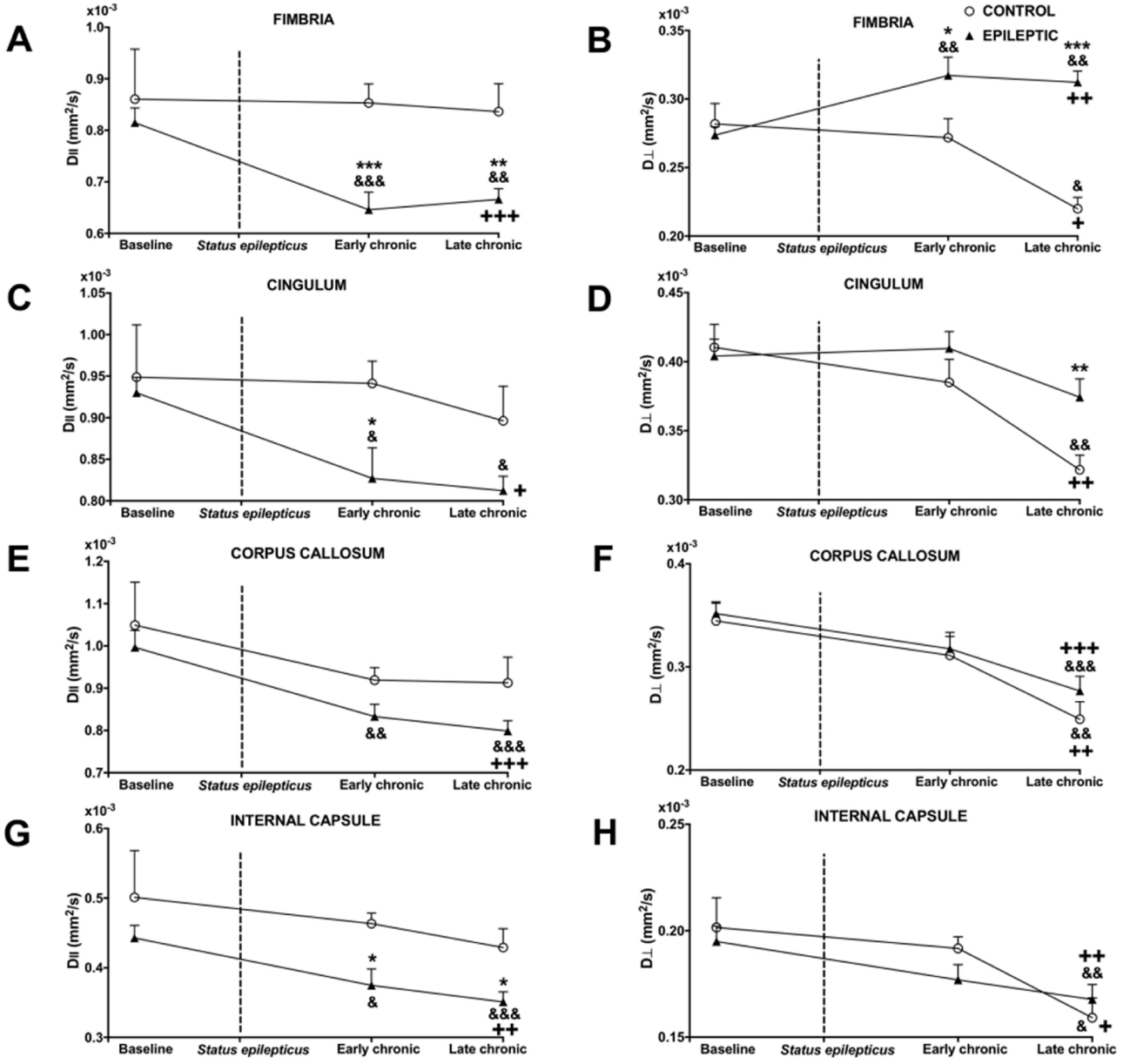

Fig. 3. Axial ($D_{\parallel}$) and radial ($D_{\perp}$) diffusivities from white matter structures of Control and Epileptic rats.
Data obtained using *in vivo* DTI. The dotted line indicates the day of the pilocarpine-induced *status epilepticus*. The epileptic group shows decreased $D_{\parallel}$ when compared to the control group (A, C, E, G). Contrary to this pattern, $D_{\perp}$ is significantly increased in the epileptic rats (B, D) or no evident changes are observed (F, H). + : repeated measures ANOVA; * : *post-hoc* between group differences; & : *post-hoc* within-group difference with respect to baseline (one, two or three symbols for $p <$ 0.05, < 0.01, and < 0.001, respectively).

0.32 ± 0.01 and Late chronic = 0.37 ± 0.013; $p < 0.01$); longitudinal changes only observed in the final time point of the control animals (↓22 %, $p < 0.01$) (Fig. 3D).

Fig. 2E shows differences of FA of corpus callosum between groups that were present at the second post-*SE* evaluation (Baseline = 0.56 ± 0.021; Late chronic = 0.59 ± 0.018; $p < 0.05$). Moreover, control and epileptic groups showed no longitudinal changes. Regarding ADC, only longitudinal changes in the experimental group were observed at both time points (Early chronic = ↓15 %, $p < 0.001$; Late chronic = ↓22 %, $p < 0.001$) (Fig. 2F). D∥ only showed longitudinally significant differences in the epileptic animals (Early chronic = ↓16 %, $p < 0.01$; Late chronic = ↓20 %, $p < 0.001$) (Fig. 3E). In the case of D⊥, only longitudinal changes were observed in control (Late chronic = ↓28 %, $p < 0.01$) and experimental animals (Late chronic = ↓21 %, $p < 0.001$) (Fig. 3F).

Similar to the other three white matter structures evaluated, the internal capsule also showed significantly decreased FA values in the epileptic animals when compared to the control group (Baseline = 0.5 ± 0.015; Early chronic = 0.45 ± 0.019, $p < 0.05$; Late chronic = 0.46±0.02, $p < 0.01$) (Fig. 2G). In the case of ADC, differences between groups were observed (Baseline = 0.28 ± 0.012; Early chronic = 0.24 ± 0.011, $p < 0.05$); longitudinal changes were only detected in the experimental group (Early chronic = ↓14 %, $p < 0.01$; Late chronic = ↓19 %, $p < 0.001$) (Fig. 2H). D∥ also showed differences between groups (Baseline = 0.44 ± 0.018; Early chronic = 0.37 ± 0.023, $p < 0.05$; Late chronic = 0.35±0.014, $p < 0.05$); longitudinal changes were only observed in the epileptic animals (Early chronic = ↓15 %, $p < 0.05$; Late chronic = ↓21 %, $p < 0.001$) (Fig. 3G). In contrast, D⊥ only showed the longitudinal ones in both groups (Control Late chronic = ↓21 %, $p < 0.05$; Epileptic Late chronic = ↓14 %, $p < 0.01$) (Fig. 3H).

3.3.2. *Gray matter structures*

In the dorsal hippocampus, epileptic animals showed a significantly increased FA value at the second post-*SE* evaluation when compared to the control group (Control = 0.25 ± 0.014; Epileptic = 0.29 ± 0.014; $p < 0.05$) (Fig. 4A). Neither ADC (Fig. 4B) nor D∥ or D⊥ (Fig. 5A and B) changes between groups were detected; longitudinally, only D⊥ changes were described in the Epileptic group while comparing Baseline *vs* Late chronic (↓8 %; $p < 0.01$) (Fig. 5B).

In CA3, no statistically significant changes in FA (Fig. 4C), ADC (Fig. 4D), D∥, or D⊥ (Fig. 5C and 5D) were observed between groups. However, ADC and D⊥ showed longitudinal changes in the Epileptic group throughout the experiment (reductions between 6% and 8%; $p < 0.05$) (Figs. 4D and 5D, respectively).

While examining the FA values of the dentate gyrus, the epileptic animals showed a significant increase with respect to the control group at 64 days post-*SE* evaluation (Baseline = 0.27 ± 0.023; Late chronic =

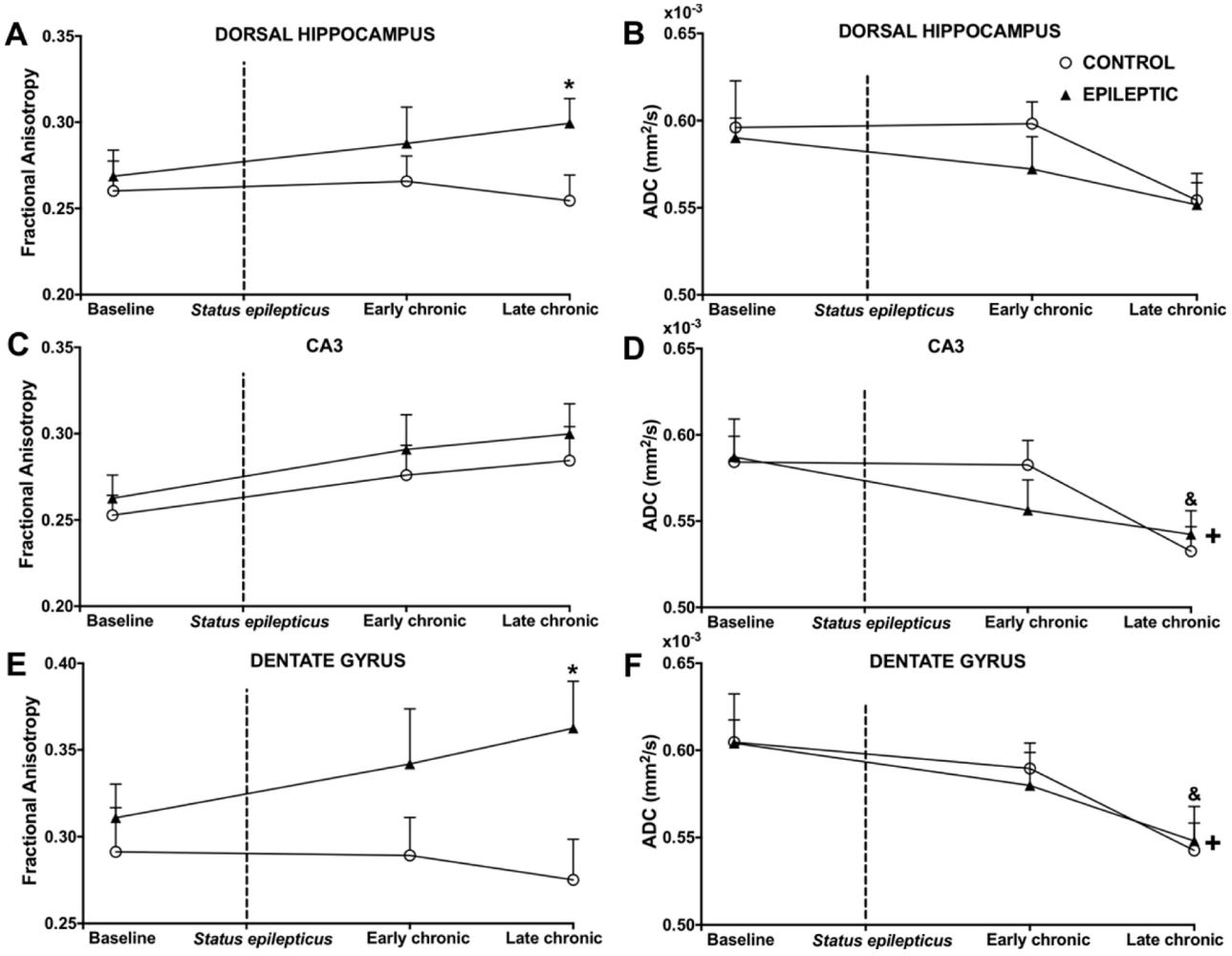

Fig. 4. Fractional anisotropy (FA) and apparent diffusion coefficient (ADC) values from gray matter structures of Control and Epileptic rats. Data obtained using *in vivo* DTI. The dotted line indicates the day of the pilocarpine-induced *status epilepticus*. The epileptic group only shows significantly increased FA values when compared to the control group in dorsal hippocampus (A) and dentate gyrus (E) at the final time point. Such differences are not so evident when comparing ADC values between groups (B, D, F). + : repeated measures ANOVA; * : *post-hoc* between group differences; & : *post-hoc* within-group difference with respect to baseline (one symbol for $p < 0.05$).

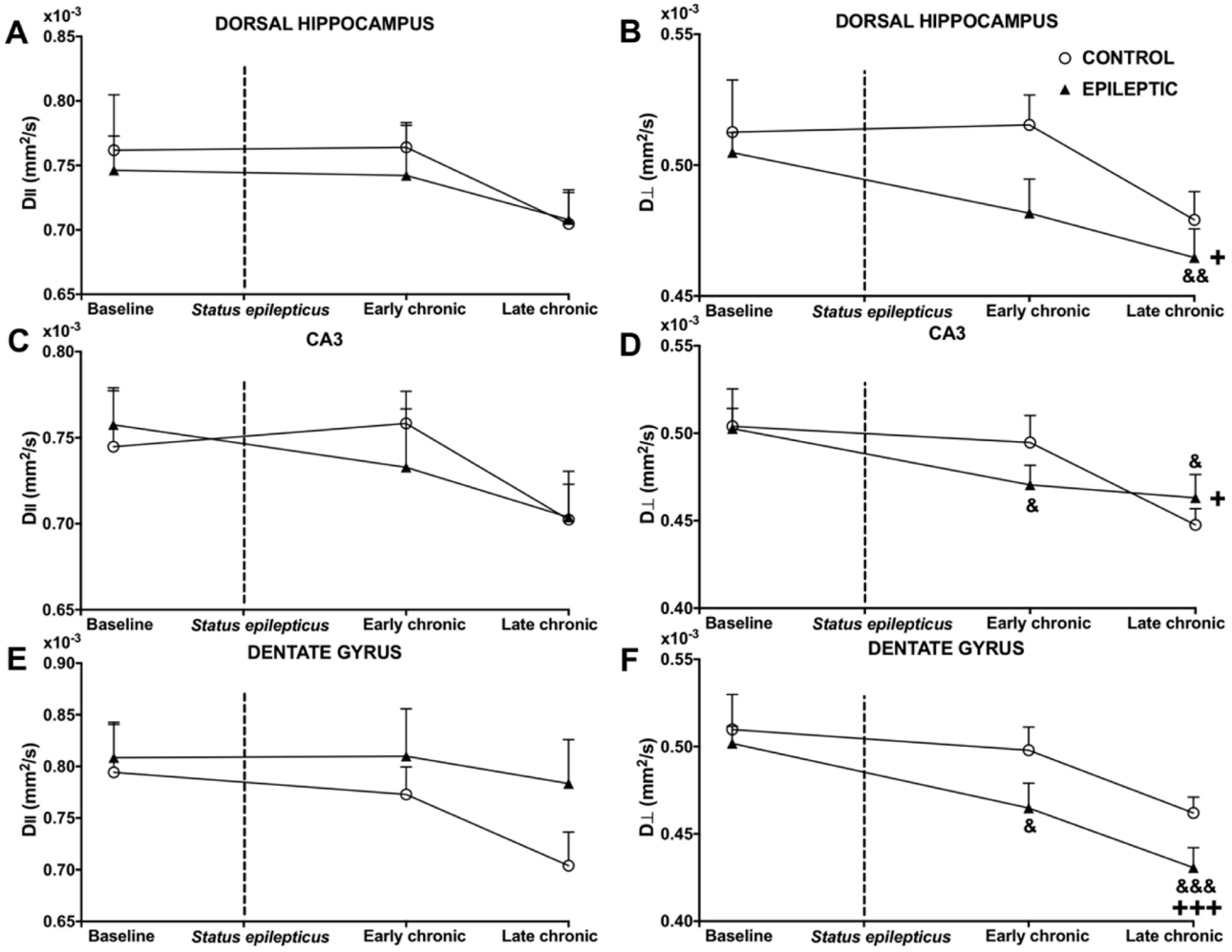

Fig. 5. Axial (D‖) and radial (D⊥) diffusivities from gray matter structures of Control and Epileptic rats.
Data obtained using *in vivo* DTI. The dotted line indicates the day of the pilocarpine-induced *status epilepticus*. No D‖ or D⊥ changes between groups are observed. In some cases, only longitudinal changes while evaluating D⊥ values of the epileptic animals (B, D, F). + : repeated measures ANOVA; * : *post-hoc* between group differences; & : *post-hoc* within-group difference with respect to baseline (one, two or three symbols for $p < 0.05$, < 0.01, and <0.001, respectively).

0.36 ± 0.027; $p < 0.05$). Similar to dorsal hippocampus and CA3, no longitudinal changes were observed (Fig. 4E). In the case of ADC, no differences between groups were detected; longitudinally, the epileptic animals showed a significant decrease at the third time point (↓9%; $p < 0.05$) (Fig. 4F). D‖ post-*SE* values remained unchanged when compared to the Baseline time point throughout the experiment (Fig. 5E). However, a significant decrease in the D⊥ of the epileptic animals was observed at Early (↓7 %; $p < 0.05$) and Late chronic (↓14 %; $p < 0.001$) (Fig. 5F).

3.4. Pilocarpine-induced histological changes

The observation of Klüver-Barrera-stained sections revealed considerable damage to the hippocampus of epileptic animals (Fig. 6D–F) compared to non-epileptic controls (Fig. 6A–C). In epileptic animals, reduction of pyramidal layer thickness was evident in CA1 and CA3 (Fig. 6D–F), together with a dispersion pattern of the remnant cells. In addition, the considerable neuronal death observed in CA3 induced the presence of several pyknotic cells (Fig. 6F).

While comparing the fimbria of both groups, an evident morphological change was observed in the epileptic group. In the case of control animals, their fimbria showed a well-delimited rectangular shape with rounded edges (Fig. 6G). On the other hand, epileptic animals presented an elongated, triangular fimbria (Fig. 6J). Moreover, Fig. 6H and I show that control subjects have a dense and homogeneous fibrillar pattern, with few interspersed glial cells. Such a pattern dramatically changes in the epileptic group, with lower fiber density and noticeably higher glial cell density (Fig. 6K and L).

4. Discussion

We demonstrate tissue abnormalities that change over time following *SE* in key gray and white matter structures relevant to the initiation and propagation of seizures originating in the temporal lobe.

The fimbria-fornix, a white matter tract bundle containing hippocampal afferent and efferent connections [29,30], has shown abnormalities in individuals with TLE [14,35,36] and in animal models of chronic TLE [9,25]. In our current study, this structure showed the largest diffusivity abnormalities following *SE,* namely reduced FA due to reduced D‖ and increased D⊥. This diffusion pattern is highly suggestive of axonal degeneration [10,33,34], and in sharp contrast with the high anisotropy seen in intact white matter with highly coherent axons, which facilitates diffusivity parallel to the direction of axons while hindering diffusion perpendicular to them. This histopathological phenomenon is expected as a result of the loss of pyramidal cells in the hippocampus after *SE*. Indeed, our experimental model induced bilateral hippocampal damage, with concomitant bilateral fimbria-fornix diffusion alterations. DTI of the fimbria-fornix proved to be more sensitive to

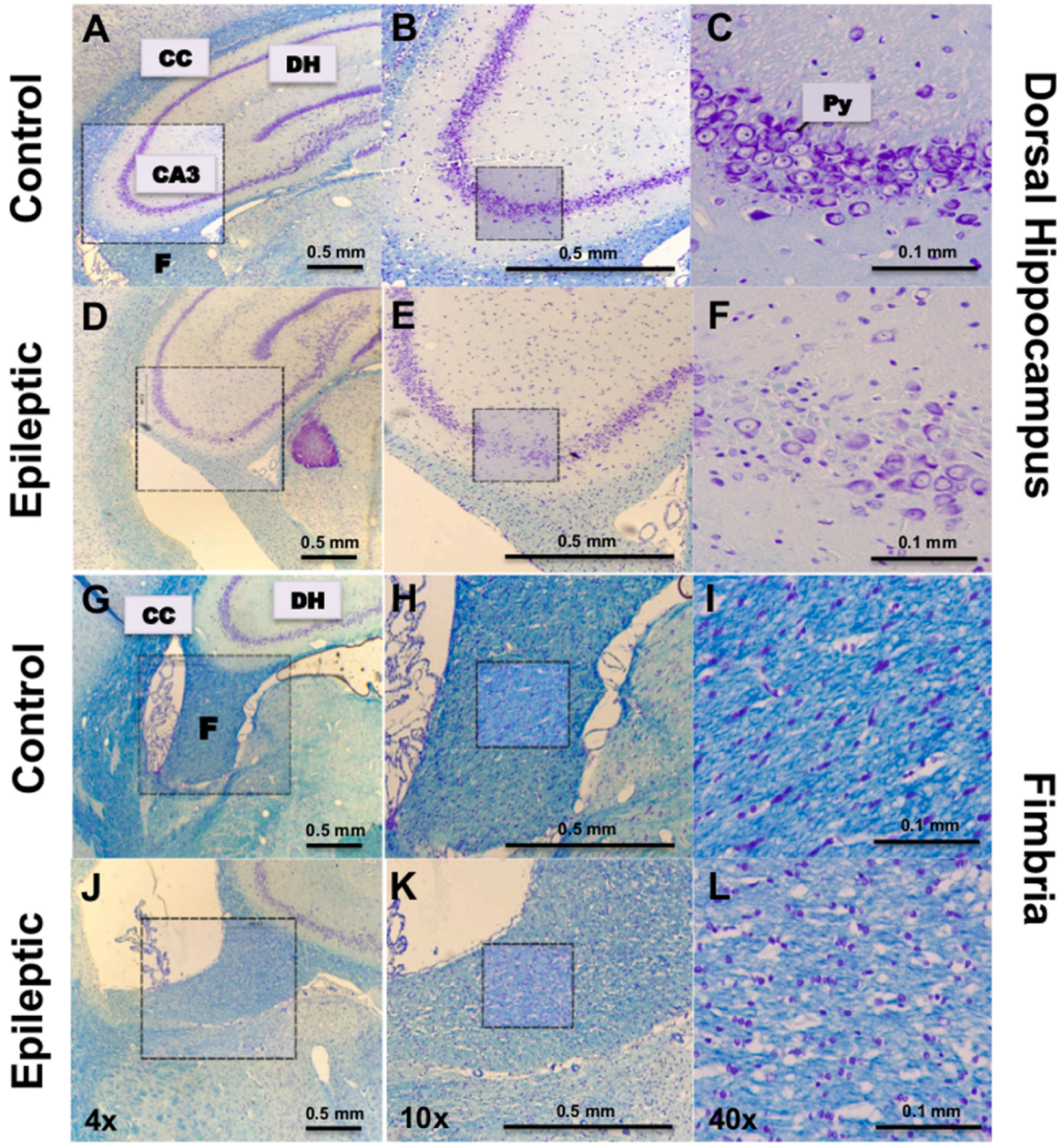

Fig. 6. Klüver-Barrera-stained sections through dorsal hippocampus and fimbria.
Status epilepticus results in structural changes in the epileptic rats (D-F and J-L). Evident cell damage, with decrease of the thickness of the pyramidal layer (D-F). Abbreviations: CC, corpus callosum; DH, dorsal hippocampus; Py, pyramidal; F, fimbria.

detect down-stream effects of hippocampal changes than measurements of the hippocampus itself. Other groups have shown similar bilateral diffusion abnormalities of the fimbria-fornix in post-*SE* animal models of TLE [5,18], and bilateral fornix alterations related to *SE* have even been demonstrated in humans [35]. However, it is still unclear why patients with unilateral mesial temporal sclerosis have bilateral diffusion abnormalities of the fornix [10,31], even after clear unilateral mesial temporal sclerosis, and in the absence of *SE*. Since DTI cannot distinguish between afferent and efferent fibers, it is impossible to establish the integrity of septo-hippocampal fibers, which may play an important role in epileptogenesis [36,37].

The dynamic ADC fluctuations have also been implicated in the pathophysiological evolution of certain brain regions in prolonged seizures or *SE*. Clinically, Szabo et al. [38] reported a peri-ictal ADC decrease in patients with complex partial *SE* at the epileptogenic region and the subcortical areas of propagation. Experimental *SE* models using kainic acid [39,40] or pilocarpine [41,42] have also shown ADC decreases. In the case of kainic acid, such decreases may last 1–3 days and then return to near-control levels by 7 days. Some experimental studies have suggested that reduced ADC values are attributable to cytotoxic intracellular edema [43] which restricts motion of intracellular water due to several factors [43,44]. Other authors also attribute reduction of ADC to macrophage, microglial and astrocytic proliferation [45]. Once in the chronic stage, neuronal cell loss and secondary gliosis [39–42,45] lead to an increase in ADC values, as the water diffuses more freely due to the structural disruption [46,47]. In our case, no differences were observed between groups while analyzing fimbria ADC values longitudinally. Although disruption of myelin and axons might increase the mean diffusivity of water molecules, glial proliferation and an accumulation of cellular debris from the breakdown of axons may hinder water molecule motion, preserving the global effect of diffusion in the affected pathways [33,48].

While the cingulum showed FA reductions similar to those of the fimbria-fornix, the underlying pattern was dissimilar, with FA of the cingulum driven mostly by reductions of D∥, while that of the fimbria-fornix was attributable to both reduced D∥ and increased D⊥. D⊥ of the cingulum was increased in this study at 64 days post-*SE*. There have been previous reports of reduced FA of the cingulum in TLE patients, similar to the abnormal pattern seen here 64 days post-*SE*, consisting of reduced FA due to increased D⊥ [10,31,49,50]. Following surgery in TLE patients, there are further abnormalities of the cingulum, likely due to Wallerian degeneration of efferent tracts arising from the resected temporal lobe [10,31,49,50]. Considering that the cingulum is a primary fascicle of the limbic system that lacks a direct connection to the hippocampus, mechanisms other than axonal degeneration may be responsible for the observed changes. Clinically detectable seizures are the result of long-lasting epileptogenic processes. Therefore, during the period preceding clinically detectable seizures, it is possible that abnormal subclinical repetitive electrical discharges through maturing axons may disturb normal myelin formation, leading to subsequent axonal damage and degeneration. This is in line with the possibility that anterior temporal white matter changes may be a side effect of early onset epileptogenic discharges and subsequent persistent seizures [51].

White matter changes in mesial TLE have been reported in multiple DTI studies. Such effects are mainly reflected as a FA reduction in ipsilateral temporal lobe white matter and extra-temporal structures such as corpus callosum and internal capsule [12,31,52–54]. These results show generalized brain damage rather than a simple alteration of the commissural fibers connecting both temporal lobes. However, FA increases can be observed after successful surgical procedures, reflecting the possibility of structural reorganization, especially in the contralateral hemisphere [54,55,57]. Similarly, van Eijsden et al. [18] reported that pilocarpine-induced *SE* in juvenile rats causes significant white matter pathology in the medial corpus callosum, persisting for several weeks, and followed by partial recovery.

Our results show that both non-limbic white matter structures have a pattern of abnormalities similar to that seen in the cingulum (and different from the fimbria-fornix), characterized by reductions of D∥ as early as 24 days post-*SE*, with D⊥ showing an increase only in the latest time point studied. These changes could be the consequence of an altered myelination process related to axonal damage, alterations of membrane permeability, and reduced neuronal density; all induced by a constant propagation of the epileptic activity [11,12,17,18,52].

Diffusion abnormalities of dentate gyrus could be attributable to mossy fiber sprouting, the main characteristic of hippocampal sclerosis, and responsible for generating abnormal neuronal circuits and hyperexcitability [56]. Similar to the diffusion alterations observed in the fimbria-fornix, this sprouting is only observed in individuals developing spontaneous recurrent seizures [5], and its detection correlates to the frequency and severity of such seizures. Gliosis and neurodegeneration have been discarded as responsible for inducing changes of diffusion anisotropy [5]. Although increases in the anisotropy of the dentate gyrus have been previously reported during the chronic stage of epileptogenesis [19], we did not observe any progressive pattern. The dramatic histological changes observed in CA3 show its vulnerability when exposed to induced *SE* and subsequent spontaneous recurrent seizures. Chronic diffusion changes are related to diffusion anisotropy in the reorganization of myelinated axons and mossy fiber sprouting [7,19]. Despite previous reports, our results did not reveal any significant difference of FA values between time points, likely due to our reduced resolution that made delineation of CA3 difficult.

There are limitations to our current study. First, animals were only imaged before *SE* and at two different time points after it. We may therefore have missed tissue abnormalities present at specific moments during epileptogenesis. Previous reports have shown that hippocampal diffusion abnormalities can be detected as early as eight days following *SE* [7,19]. Nonetheless, the temporal evolution of diffusion changes may be even more complex, as evidenced with the MSO model of TLE, with particular changes occurring in the first few days. Second, while spatial resolution was adequate in-plane, the thick slices acquired likely resulted in partial volume averaging. Our two-dimensional acquisition also complicated volume registration to an atlas for automatic segmentation of the structures of interest, which was performed manually. Third, the tensor model is known to have several limitations for the study of white matter with complex configurations [57]. While this technical shortcoming may be of little consequence in the white matter structures we studied (composed of a single fiber population), it impacts measurements of gray matter, where advanced methods are warranted [58]. Finally, our histological observations confirmed white and gray matter damage, yet they were qualitative and not designed to fully characterize the biological factors driving diffusion changes [7,19], and only available for the late chronic time point.

5. Conclusion

We provide evidence of time-dependent diffusion changes in gray and white matter in a rodent model of TLE. The characterization of tissue damage over time in this often-used animal model provides a non-destructive test bed to evaluate the impact of different experimental approaches to minimize tissue damage and modulate epileptogenesis.

Funding sources

Funding for this work was provided by the Mexican Council of Science and Technology (CONACYT, grants C1782 for LC and 476271 for LMB) and UNAM-DGAPA-PAPIIT (IA200719 for HLM and AG200117 for LC).

Author contributions

HLM and LC made substantial contributions to conception and design.

HLM, LMB, and LC made substantial contributions to acquisition of data.

HLM, LMB, and LC made substantial contributions to analysis and interpretation of data.

HLM and LC were involved in drafting the manuscript and revising it critically.

Declaration of Competing Interest

The authors report no declarations of interest.

Acknowledgements

Imaging was performed at the National Laboratory for Magnetic Resonance Imaging (CONACYT, UNAM, CIMAT, UAQ). We thank Dr. Deisy Gasca-Martinez, responsible for the Behavioral Unit. We also thank the personnel at the Animal Facility and Dr. Juan Ortiz-Retana for assistance during MRI acquisition; Leticia Castillo Heredia, Gema Martinez Cabrera, Ericka de los Rios, and Nydia Hernandez Rios for their help with the histological procedures; Leopoldo Gonzalez Santos for technical assistance. Jessica Gonzalez-Norris for proof-reading and editing our manuscript.

Appendix A. Supplementary data

Supplementary data associated with this article can be found, in the online version, at https://doi.org/10.1016/j.seizure.2021.02.011.

References

[1] Basser PJ, Mattiello J, LeBihan D. MR diffusion tensor spectroscopy and imaging. Biophys J 1994;66(1):259–67. https://doi.org/10.1016/S0006-3495(94)80775-1.

[2] Coras R, Milesi G, Zucca I, Mastropietro A, Scotti A, Figini M, et al. 7T MRI features in control human hippocampus and hippocampal sclerosis: an ex vivo study with histologic correlations. Epilepsia 2014;55(12):2003–16. https://doi.org/10.1111/epi.12828.
[3] Rodriguez-Cruces R, Concha L. White matter in temporal lobe epilepsy: clinico-pathological correlates of water diffusion abnormalities. Quant Imaging Med Surg 2015;5(2):264–78. https://doi.org/10.3978/j.issn.2223-4292.2015.02.06.
[4] Laitinen T, Sierra A, Pitkanen A, Grohn O. Diffusion tensor MRI of axonal plasticity in the rat hippocampus. Neuroimage 2010;51(2):521–30. https://doi.org/10.1016/j.neuroimage.2010.02.077.
[5] Parekh MB, Carney PR, Sepulveda H, Norman W, King M, Mareci TH. Early MR diffusion and relaxation changes in the parahippocampal gyrus precede the onset of spontaneous seizures in an animal model of chronic limbic epilepsy. Exp Neurol 2010;224(1):258–70. https://doi.org/10.1016/j.expneurol.2010.03.031.
[6] Sierra A, Laitinen T, Grohn O, Pitkanen A. Diffusion tensor imaging of hippocampal network plasticity. Brain Struct Funct 2015;220(2):781–801. https://doi.org/10.1007/s00429-013-0683-7.
[7] Janz P, Schwaderlapp N, Heining K, Häussler U, Korvink JG, von Elverfeldt D, et al. Early tissue damage and microstructural reorganization predict disease severity in experimental epilepsy. Elife 2017;6:e25742. https://doi.org/10.7554/eLife.25742.
[8] Wang H, Huang Y, Coman D, Munbodh R, Dhaher R, Zaveri HP, et al. Network evolution in mesial temporal lobe epilepsy revealed by diffusion tensor imaging. Epilepsia 2017;58(5):824–34. https://doi.org/10.1111/epi.13731.
[9] Arfanakis K, Hermann BP, Rogers BP, Carew JD, Seidenberg M, Meyerand ME. Diffusion tensor MRI in temporal lobe epilepsy. Magn Reson Imaging 2002;20(7):511–9. https://doi.org/10.1016/s0730-725x(02)00509-x.
[10] Concha L, Beaulieu C, Gross DW. Bilateral limbic diffusion abnormalities in unilateral temporal lobe epilepsy. Ann Neurol 2005;57(2):188–96. https://doi.org/10.1002/ana.20334.
[11] Concha L, Livy DJ, Beaulieu C, Wheatley BM, Gross DW. In vivo diffusion tensor imaging and histopathology of the fimbria-fornix in temporal lobe epilepsy. J Neurosci 2010;30(3):996–1002. https://doi.org/10.1523/JNEUROSCI.1619-09.2010.
[12] Gross DW, Concha L, Beaulieu C. Extratemporal white matter abnormalities in mesial temporal lobe epilepsy demonstrated with diffusion tensor imaging. Epilepsia 2006;47(8):1360–3. https://doi.org/10.1111/j.1528-1167.2006.00603.x.
[13] Schoene-Bake JC, Faber J, Trautner P, Kaaden S, Tittgemeyer M, Elger CE, et al. Widespread affections of large fiber tracts in postoperative temporal lobe epilepsy. Neuroimage 2009;46(3):569–76. https://doi.org/10.1016/j.neuroimage.2009.03.013.
[14] Otte WM, van Eijsden P, Sander JW, Duncan JS, Dijkhuizen RM, Braun KPJ. A meta-analysis of white matter changes in temporal lobe epilepsy as studied with diffusion tensor imaging. Epilepsia 2012;53(4):659–67. https://doi.org/10.1111/j.1528-1167.2012.03426.x.
[15] Hatton SN, Huynh KH, Bonilha L, Abela E, Alhusaini S, et al. White matter abnormalities across different epilepsy syndromes in adults: an ENIGMA-Epilepsy study. Brain 2020;143(8):2454–73. https://doi.org/10.1093/brain/awaa200.
[16] Miro J, Gurtubay-Antolin A, Ripolles P, Sierpowska J, Juncadella M, Fuentemilla L, et al. Interhemispheric microstructural connectivity in bitemporal lobe epilepsy with hippocampal sclerosis. Cortex 2015;67:106–21. https://doi.org/10.1016/j.cortex.2015.03.018.
[17] Vaughan DN, Raffelt D, Curwood E, Tsai MH, Tournier JD, Connelly A, et al. Tract-specific atrophy in focal epilepsy: disease, genetics, or seizures? Ann Neurol 2017;81(2):240–50. https://doi.org/10.1002/ana.24848.
[18] van Eijsden P, Otte WM, van der Hel WS, van Nieuwenhuizen O, Dijkhuizen RM, de Graaf RA, et al. In vivo diffusion tensor imaging and ex vivo histologic characterization of white matter pathology in a post-status epilepticus model of temporal lobe epilepsy. Epilepsia 2011;52(4):841–5. https://doi.org/10.1111/j.1528-1167.2011.02991.x.
[19] Salo RA, Miettinen T, Laitinen T, Grohn O, Sierra A. Diffusion tensor MRI shows progressive changes in the hippocampus and dentate gyrus after status epilepticus in rat. Histological validation with Fourier-based analysis. Neuroimage 2017;152:221–36. https://doi.org/10.1016/j.neuroimage.2017.03.003.
[20] Turski WA, Cavalheiro EA, Schwarz M, Czuczwar SJ, Kleinrok Z, Turski L. Limbic seizures produced by pilocarpine in rats: behavioural, electroencephalographic and neuropathological study. Behav Brain Res 1983;9(3):315–35. https://doi.org/10.1016/0166-4328(83)90136-5.
[21] Leite JP, Bortolotto ZA, Cavalheiro EA. Spontaneous recurrent seizures in rats: an experimental model of partial epilepsy. Neurosci Biobehav Rev 1990;14(4):511–7. https://doi.org/10.1016/s0149-7634(05)80076-4.
[22] Cavalheiro EA, Leite JP, Bortolotto ZA, Turski WA, Ikonomidou C, Turski L. Long-term effects of pilocarpine in rats: structural damage of the brain triggers kindling and spontaneous recurrent seizures. Epilepsia 1991;32(6):778–82. https://doi.org/10.1111/j.1528-1157.1991.tb05533.x.
[23] Veraart J, Novikov DS, Christiaens D, Ades-Aron B, Sijbers J, Fieremans E. Denoising of diffusion MRI using random matrix theory. Neuroimage 2016;142:394–406. https://doi.org/10.1016/j.neuroimage.2016.08.016.
[24] Tournier JD, Smith R, Raffelt D, Tabbara R, Dhollander T, Pietsch M, et al. MRtrix3: a fast, flexible and open software framework for medical image processing and visualisation. Neuroimage 2019;202:116137. https://doi.org/10.1016/j.neuroimage.2019.116137.
[25] Basser PJ, Pierpaoli C. Microstructural and physiological features of tissues elucidated by quantitative-diffusion-tensor MRI. J Magn Reson 2011;213(2):560–70. https://doi.org/10.1016/j.jmr.2011.09.022.
[26] Luna-Munguia H, Starski P, Chen W, Gliske S, Stacey WC. Control of in vivo ictogenesis via endogenous synaptic pathways. Sci Rep 2017;7(1):1311. https://doi.org/10.1038/s41598-017-01450-8.
[27] Curia G, Longo D, Biagini G, Jones RSG, Avoli M. The pilocarpine model of temporal lobe epilepsy. J Neurosci Methods 2008;172(2):143–57. https://doi.org/10.1016/j.jneumeth.2008.04.019.
[28] Goffin K, Nissinen J, Van Laere K, Pitkanen A. Cyclicity of spontaneous recurrent seizures in pilocarpine model of temporal lobe epilepsy in rat. Exp Neurol 2007;205(2):501–5. https://doi.org/10.1016/j.expneurol.2007.03.008.
[29] Mori S, Aggarwal M. In vivo magnetic resonance imaging of the human limbic white matter. Front Aging Neurosci 2014;6:321. https://doi.org/10.3389/fnagi.2014.00321.
[30] Mathiasen ML, Louch RC, Nelson AD, Dillingham CM, Aggleton JP. Trajectory of hippocampal fibres to the contralateral anterior thalamus and mammillary bodies in rats, mice, and macaque monkeys. Brain Neurosci Adv 2019:3. https://doi.org/10.1177/2398212819871205.
[31] Concha L, Beaulieu C, Collins DL, Gross DW. White-matter diffusion abnormalities in temporal-lobe epilepsy with and without mesial temporal sclerosis. J Neurol Neurosurg Psychiatry 2009;80(3):312–9. https://doi.org/10.1136/jnnp.2007.139287.
[32] Urbach H, Egger K, Rutkowski K, Nakagawa JM, Schmeiser B, Reisert M, et al. Bilateral cingulum fiber reductions in temporal lobe epilepsy with unilateral hippocampal sclerosis. Eur J Radiol 2017;94:53–7. https://doi.org/10.1016/j.ejrad.2017.07.015.
[33] Beaulieu C, Does MD, Snyder RE, Allen PS. Changes in water diffusion due to Wallerian degeneration in peripheral nerve. Magn Reson Med 1996;36(4):627–31. https://doi.org/10.1002/mrm.1910360419.
[34] George R, Griffin JW. Delayed macrophage responses and myelin clearance during Wallerian degeneration in the central nervous system: the dorsal radiculotomy model. Exp Neurol 1994;129(2):225–36. https://doi.org/10.1006/exnr.1994.1164.
[35] Gong G, Shi F, Concha L, Beaulieu C, Gross DW. Insights into the sequence of structural consequences of convulsive status epilepticus: a longitudinal MRI study. Epilepsia 2008;49(11):1941–5. https://doi.org/10.1111/j.1528-1167.2008.01666.x.
[36] Colom LV, Garcia-Hernandez A, Castañeda MT, Perez-Cordova MG, Garrido-Sanabria ER. Septo-hippocampal networks in chronically epileptic rats: potential antiepileptic effects of theta rhythm generation. J Neurophysiol 2006;95(6):3645–53. https://doi.org/10.1152/jn.00040.2006.
[37] Garrido-Sanabria ER, Castañeda MT, Banuelos C, Perez-Cordova MG, Hernandez S, Colom LV. Septal GABAergic neurons are selectively vulnerable to pilocarpine-induced status epilepticus and chronic spontaneous seizures. Neuroscience 2006;142(3):871–83. https://doi.org/10.1016/j.neuroscience.2006.06.057.
[38] Szabo K, Poepel A, Pohlmann-Eden B, Hirsch J, Back T, Sedlaczek O, et al. Diffusion-weighted and perfusion MRI demonstrates parenchymal changes in complex partial status epilepticus. Brain 2005;128(Pt 6):1369–76. https://doi.org/10.1093/brain/awh454.
[39] Nakasu Y, Nakasu S, Morikawa S, Uemura S, Inubushi T, Handa J. Diffusion-weighted MR in experimental sustained seizures elicited with kainic acid. AJNR Am J Neuroradiol 1995;16(6):1185–92.
[40] Wang Y, Majors A, Najm I, Xue M, Comair Y, Modic M, et al. Postictal alteration of sodium content and apparent diffusion coefficient in epileptic rat brain induced by kainic acid. Epilepsia 1996;37(10):1000–6. https://doi.org/10.1111/j.1528-1157.1996.tb00539.x.
[41] Fabene PF, Marzola P, Sbarbati A, Bentivoglio M. Magnetic resonance imaging of changes elicited by status epilepticus in the rat brain: difussion-weighted and T2-weighted images, regional blood volume maps, and direct correlation with tissue and cell damage. Neuroimage 2003;18(2):375–89. https://doi.org/10.1016/s1053-8119(02)00025-3.
[42] Engelhorn T, Weise J, Hammen T, Bluemcke I, Hufnagel A, Doerfler A. Early diffusion-weighted MRI predicts regional neuronal damage in generalized status epilepticus in rats treated with diazepam. Neurosci Lett 2007;417(3):275–80. https://doi.org/10.1016/j.neulet.2007.02.072.
[43] Gass A, Niendorf T, Hirsch JG. Acute and chronic changes of the apparent diffusion coefficient in neurological disorders – biophysical mechanisms and possible underlying histopathology. J Neurol Sci 2001;186(Suppl. 1):S15–23. https://doi.org/10.1016/s0022-510x(01)00487-7.
[44] Eidt S, Kendall EJ, Obenaus A. Neuronal and glial cell populations in the piriform cortex distinguished by using an approximation of Q-Space imaging after status epilepticus. AJNR Am J Neuroradiol 2004;25(7):1225–33.
[45] Wall CJ, Kendall EJ, Obenaus A. Rapid alterations in diffusion-weighted images with anatomic correlates in a rodent model of status epilepticus. AJNR Am J Neuroradiol 2000;21(10):1841–52.
[46] Yoo SY, Chang KH, Song IC, Han MH, Kwon BJ, Lee SH, et al. Apparent diffusion coefficient value of the hippocampus in patients with hippocampal sclerosis and in healthy volunteers. AJNR Am J Neuroradiol 2002;23(5):809–12.
[47] Hasegawa D, Orima H, Fujita M, Nakamura S, Takahashi K, Ohkubo S, et al. Diffusion-weighted imaging in kainic acid-induced complex partial status epilepticus in dogs. Brain Res 2003;983(1–2):115–27. https://doi.org/10.1016/s0006-8993(03)03041-5.
[48] Werring DJ, Toosy AT, Clark CA, Parker GJ, Barker GJ, Miller DH, et al. Diffusion tensor imaging can detect and quantify corticospinal tract degeneration after stroke. J Neurol Neurosurg Psychiatry 2000;69(2):269–72. https://doi.org/10.1136/jnnp.69.2.269.
[49] McDonald CR, Hagler DJ, Girard HM, Pung C, Ahmadi ME, Holland D, et al. Changes in fiber tract integrity and visual fields after anterior temporal lobectomy.

Neurology 2010;75(18):1631–8. https://doi.org/10.1212/WNL.0b013e3181fb44db.

[50] Winston G, Stretton J, Sidhu MK, Symms MR, Duncan JS. Progressive white matter changes following anterior temporal lobe resection for epilepsy. Neuroimage Clin 2013;4:190–200. https://doi.org/10.1016/j.nicl.2013.12.004.

[51] OEMG Schijns, Bien CG, Majores M, von Lehe M, Urbach H, Becker A, et al. Presence of temporal gray-white matter abnormalities does not influence epilepsy surgery outcome in temporal lobe epilepsy with hippocampal sclerosis. Neurosurgery 2011;68(1):98–106. https://doi.org/10.1227/NEU.0b013e3181fc60ff.

[52] Concha L, Beaulieu C, Wheatley BM, Gross DW. Bilateral white matter diffusion changes persist after epilepsy surgery. Epilepsia 2007;48(5):931–40. https://doi.org/10.1111/j.1528-1167.2007.01006.x.

[53] Scanlon C, Mueller SG, Cheong I, Hartig M, Weiner MW, Laxer KD. Grey and white matter abnormalities in temporal lobe epilepsy with and without mesial temporal sclerosis. J Neurol 2013;260(9):2320–9. https://doi.org/10.1007/s00415-013-6974-3.

[54] Li W, An D, Tong X, Liu W, Xiao F, Ren J, et al. Different patterns of white matter changes after successful surgery of mesial temporal lobe epilepsy. Neuroimage Clin 2019;21:101631. https://doi.org/10.1016/j.nicl.2018.101631.

[55] Yogarajah M, Focke NK, Bonelli SB, Thompson P, Vollmar C, McEvoy AW, et al. The structural plasticity of white matter networks following anterior temporal lobe resection. Brain 2010;133(8):2348–64. https://doi.org/10.1093/brain/awq175.

[56] Scharfman HE, Goodman JH, Sollas AL. Granule-like neurons at the hilar/CA3 border after status epilepticus and their synchrony with area CA3 pyramidal cells: functional implications of seizure-induced neurogenesis. J Neurosci 2000;20(16):6144–58. https://doi.org/10.1523/JNEUROSCI.20-16-06144.2000.

[57] Tournier JD, Mori S, Leemans A. Diffusion tensor imaging and beyond. Magn Reson Med 2011;65(6):1532–56. https://doi.org/10.1002/mrm.22924.

[58] Assaf Y. Imaging laminar structures in the gray matter with diffusion MRI. Neuroimage 2019;197:677–88. https://doi.org/10.1016/j.neuroimage.2017.12.096.